Electrochemical Oxidation of Anastrozole over a BDD Electrode: Role of Operating Parameters and Water Matrix

Rebecca Dhawle [1] , Zacharias Frontistis [2,3] and Dionissios Mantzavinos [1,*]

1 Department of Chemical Engineering, University of Patras, 26504 Patras, Greece
2 Department of Chemical Engineering, University of Western Macedonia, 50132 Kozani, Greece
3 School of Sciences and Engineering, University of Nicosia, Nicosia 2417, Cyprus
* Correspondence: mantzavinos@chemeng.upatras.gr

Abstract: The electrochemical oxidation (EO) of the breast-cancer drug anastrozole (ANZ) is studied in this work. The role of various operating parameters, such as current density (6.25 and 12.5 mA cm^{-2}), pH (3–10), ANZ concentration (0.5–2 mg L^{-1}), nature of supporting electrolytes, water composition, and water matrix, have been evaluated. ANZ removal of 82.4% was achieved at 1 mg L^{-1} initial concentration after 90 min of reaction at 6.25 mA cm^{-2} and 0.1 M Na$_2$SO$_4$. The degradation follows pseudo-first-order kinetics with the apparent rate constant, k$_{app}$, equal to 0.022 min^{-1}. The k$_{app}$ increases with increasing current density and decreasing solution pH. The addition of chloride in the range 0–250 mg L^{-1} positively affects the removal of ANZ. However, chloride concentrations above 250 mg L^{-1} have a detrimental effect. The presence of bicarbonate or organic matter has a slightly negative but not significant effect on the process. The EO of ANZ is compared to its degradation by solar photo-Fenton, and a preliminary economic analysis is also performed.

Keywords: anastrozole; BDD; electrochemical oxidation; micropollutants; AOPs; cancer drug
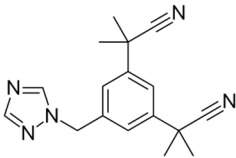
1. Introduction

Breast cancer is one of the most prominent reasons for death across the globe [1]. According to WHO reports, there were over 2 million diagnosed cases of breast cancer and 68,500 deaths reported in the year 2020 [2]. As a result, numerous aromatase-inhibiting drugs are prescribed to suppress the formation of tumors in post-menopausal women. Anastrozole (ANZ), whose main features are shown in Table 1, is a third-generation non-steroidal drug that can potentially decrease global deaths due to breast cancer [3]. Available on the market since 1995 and approved by 79 countries, ANZ is on the WHO's list of Essential Medicines [4,5]. It is categorized as a non-steroidal benzotriazole, available in the form of oral tablets [6]. With over 3 million prescriptions of ANZ handed out in 2020 in the US alone, it is a readily available drug [7]. ANZ is absorbed by the body, metabolized, and excreted out by the kidneys through urine with more than 10% of the drug intact [4,8]; thus, this drug and its metabolites enter the water streams.

Anti-cancer drugs detected in water matrices, even at very low concentrations, have the potential to cause genotoxicity, mutagenicity, and carcinogenicity [9]. ANZ and its metabolites have been detected in the concentration range of ng L^{-1} in real water matrices, such as hospital and municipal wastewater treatment plant effluents [10]. Their detection in the effluent samples suggests that the existing water treatment plants are not equipped to remove contaminants at such low concentrations.

In recent years, advanced oxidation processes (AOPs) have received considerable attention for their ability to generate highly oxidative reactive oxygen species (ROS). These ROS, such as hydroxyl ($\cdot$OH) radicals and sulfate (SO$_4-\cdot$) radicals, break down complex toxic molecules into less toxic smaller fragments, eventually resulting in their complete mineralization to carbon dioxide and water [11]. Electrochemical AOPs (e-AOPs) exhibit

a considerable advantage over other AOPs due to their non-selectivity towards organic compounds [12,13], the complete elimination without the need for additional chemicals [14], and sludge or concentrate formation via simple and clean treatment methods [15]. In an e-AOP, the organic pollutant is oxidized either (i) directly by the ROS generated at the surface of the electrode or (ii) indirectly by the ROS generated via water oxidation. Electrolysis further generates some additional ROS, enhancing the process efficiency by diffusion through the bulk and, thus, overcoming mass transfer limitation issues [16]. Electrochemical oxidation is one of the most used e-AOPs, where ·OH radicals are generated on the surface of the anode. Depending on the composition of the matrix and the electrode material, several other radicals might be generated, which can further favor anodic oxidation.

Table 1. Anastrozole characteristics.

PARAMETERS	DESCRIPTION
COMMERCIAL NAME	Anastrozole
IUPAC NAME	2,2′-[5-(1*H*-1,2,4-triazol-1-ylmethyl)-1,3-phenylene]bis(2-methylpropanenitrile)
MOLECULAR FORMULA	$C_{17}H_{19}N_5$
DRUG CLASS	Aromatase Inhibitor
STRUCTURE	
MOLECULAR MASS	293.374 g mol^{-1}
CAS NUMBER	120511-73-1
APPLICATION	Treatment of Breast Cancer

Different types of electrodes, such as screen-printed electrodes, mixed metal oxides (MMOs), dimensionally stable anodes (DSAs), and 3D or particle electrodes, have been used for environmental applications. Boron-doped diamond (BDD) electrodes are considered the ideal non-active electrodes, and they are the most used anodes for electrochemical oxidation [17] due to their wide potential window and their enhanced ability to produce ROS compared to other anode materials. Consequently, the organic pollutants are effectively removed by mineralization [18]. However, several parameters, such as the composition of the water matrix, the concentration of the electrolytes, and the pH, play a key role in the efficiency of the process. In general, the efficiency is expected to decrease as the complexity of the water matrix increases [19].

Only one published work is available, showing the removal of ANZ by a solar photo-Fenton process [20], making this the second work on ANZ removal and the only study documenting the removal of ANZ via an e-AOP. In this work, the removal of 1 mg L^{-1} is studied while evaluating the effects of several operating parameters such as current density, nature of supporting electrolyte, matrix composition, and pH, amongst others.

2. Materials and Methods

2.1. Chemicals

Anastrozole ($C_{17}H_{19}N_5$) was purchased from Interchim, Montluçon, France. Sodium sulfate (Na_2SO_4) was acquired from Lachner, Neratovice, Czech Republic. Sodium persulfate ($Na_2S_2O_8$) was bought from Scharlau Chemicals, Istanbul, Turkey. Sodium hydroxide (NaOH) was purchased from Penta Chemicals, Prague, Czech Republic. HPLC grade methanol (CH_3OH) and acetonitrile (CH3CN) were supplied by Fischer Scientific, Pittsburgh, PA, USA. Sodium chloride (NaCl), sodium bicarbonate (Na_2CO_3), sulfuric acid

(H_2SO_4), benzoic acid, tert-butanol, and humic acid were supplied by Sigma-Aldrich, Saint Louis, MO, USA. The boron-doped diamond electrode (B/C = 1000 ppm) was purchased from Adamant Technologies SA, La Chaux-de-Fonds, Switzerland. The current was supplied using a PeakTech 1890 (Linthicum, MD, USA) programmable power supply unit. A water purification unit (Millipore Corp., Billerica, MA, USA), providing water at a resistance of 18.2 mΩ cm, was used to supply ultrapure water. Commercially available bottled water and the secondary effluent from a hospital wastewater treatment plant in Patras, Greece, were also used. The composition of the bottled water and wastewater used are provided in Table 2.

Table 2. Composition of bottled water and secondary treated wastewater.

Water Matrix:	Bottled Water (BW)	Wastewater (WW)
Contents	Concentration (mg L^{-1})	Concentration (mg L^{-1})
HCO_3^-	273.9	278
Cl^-	3.8	262
NO_2^-	0	n.d
SO_4^-	7.9	0
NO_3^-	1	n.d
PO_4^-	n.d	14.9
F^-	0.07	0
Ca^{2+}	75.5	112
Mg^{2+}	5.1	n.d
Na^+	2.1	n.d
K^+	0.6	n.d
TDS	254	n.d
TSS	n.d	22
TOC	<1	2.5
COD	n.d	48.5

n.d: Not determined.

2.2. Experimental Set-Up

A rectangular plexiglass reactor of 200 mL capacity was used to perform the electrochemical experiments in batch mode at room temperature. A boron-doped diamond electrode was used as the anode and a stainless-steel plate as the cathode. The active surface area of both electrodes used was 16 cm^2. The reactor was open to the air, and the two electrodes were kept opposite each other, 9 cm apart. A magnetic stirrer was used continuously throughout the process to enhance mass transfer. The electrodes were connected to the external power supply unit. All the experiments were performed under galvanostatic conditions; 0.1 M Na_2SO_4 was used as the electrolyte, except in an experiment where 0.1 M NaCl was used. The pH was monitored at the beginning and the end of each experiment using a pH/Ion meter (SevenCompact S220, Mettler Toledo, Columbus, OH, USA). pH adjustments were made without any buffering using appropriate quantities of 1 M NaOH (for basic conditions) or 1 M H_2SO_4 (for acidic conditions); 1.2 mL of samples were collected at regular time intervals, quenched with 0.3 mL of methanol, filtered, and analyzed using high-pressure liquid chromatography (HPLC).

2.3. Analytical Methods

A Waters Alliance 2695 high-pressure liquid chromatography system was used to measure the concentration of ANZ. ANZ was eluted with a mobile phase consisting of 60% water and 40% acetonitrile and detected at 210 nm with a photodiode array detector within the HPLC system.

The determination of the ANZ diffusion coefficient was conducted using an Autolab potentiostat PGSTAT128N (Utrecht, The Netherlands). Chronoamperometry was performed at a fixed potential of 1 V over 45 s in solutions containing different concentrations of ANZ, according to the work of Fotouhi et al. [21]. From the slope of the current with

$t^{-1/2}$ at different ANZ concentrations, the diffusion coefficient was estimated using the Cottrel equation with a mean value equal to 3.1×10^{-7} cm^2/s.

3. Results and Discussion

3.1. Effect of Current Density

The current density (j) effect on the electrochemical removal of 1 mg L^{-1} ANZ in 0.1 M Na$_2$SO$_4$ is shown in Figure 1. In total, 82.4% and 97.5% of ANZ were removed at the current densities of 6.25 and 12.5 mA cm^{-2}, respectively. Increased current density has a positive influence on the process that can be attributed to the increased electro-generation of $\cdot$OH radicals on the surface of the BDD anode, as per Equation (1) [22,23], which accelerates the abatement of ANZ.

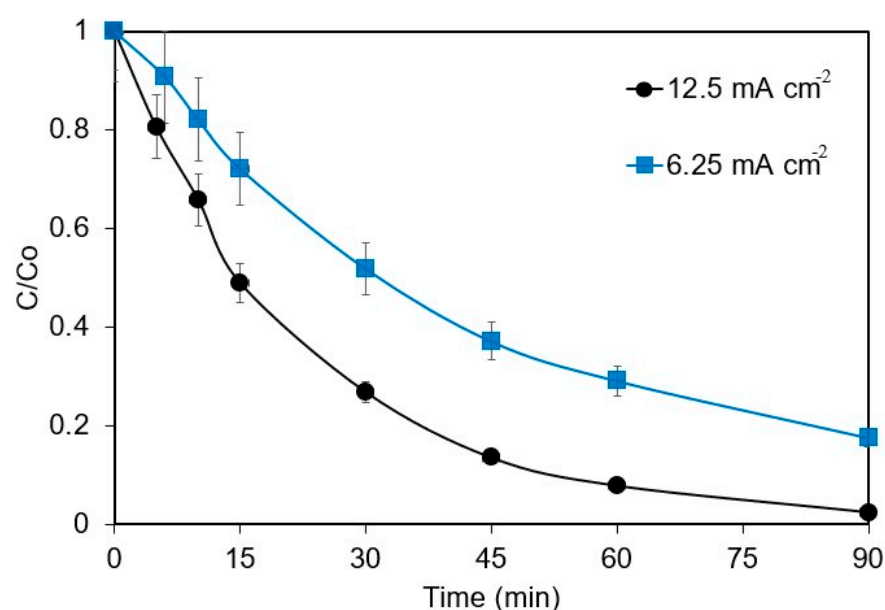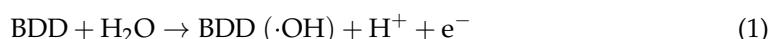$$BDD + H_2O \rightarrow BDD \, (\cdot OH) + H^+ + e^- \tag{1}$$

Figure 1. Effect of current density on ANZ removal for [ANZ]$_o$ = 1 mg L^{-1}, [Na$_2$SO$_4$] = 0.1 M, and pH = 6.2.

Considering that oxidation by hydroxyl radicals is the main mechanism of ANZ removal and neglecting the direct oxidation and adsorption effect of ANZ on the BDD for low concentrations of ANZ, the pseudo-first-order kinetics can be represented by Equation (2) [17,24].

$$-\frac{d[ANZ]}{dt} = k_{app}[ANZ] \longleftrightarrow \ln \frac{[ANZ]}{[ANZ]_o} = -k_{app}t \tag{2}$$

where k_{app} is the apparent rate constant that embodies the almost constant concentration of $\cdot$OH radicals. The k_{app} for both current densities was computed by plotting the logarithmic decay of the ANZ concentration (ln $\frac{ANZ}{ANZ_o}$) against time (t). The k_{app} values of 0.022 and 0.0422 min^{-1} were obtained for the current densities of 6.25 and 12.5 mA cm^{-2}, respectively, indicating a two-fold increase in the k_{app} values upon doubling the current density. The results obtained in this work are similar to those reported by Pueyo et al. [19] for the removal of butyl paraben, wherein complete removal was obtained in 5 min at 107–143 mA cm^{-2}, 10 min at 71 mA cm^{-2}, and 15 min at 50 mA cm^{-2}. A study on the degradation of ampicillin also showed increased k_{app} values from 0.08 to 0.6 min^{-1} on increasing current density from 5 to 110 mA cm^{-2} [24]. However, higher current densities might not always be favorable due to (i) the parasitic reaction of oxygen evolution and (ii) the side reactions producing other radicals with lower oxidizing capacity and, therefore, reducing the mineralization efficiency drastically [25]. Better removal rates have been reported with low current

densities and low energy consumption, suggesting that current densities of 100 mA cm^{-2} are ideal for removing organic pollutants [26].

3.2. Estimation of the Steady State Concentration of Hydroxyl Radicals

It is well known that BDD is considered an ideal non-active electrode due to its ability to produce physisorbed hydroxyl radicals [16,27].

To further confirm the dominant role of ·OH in the electrochemical oxidation of ANZ, an experiment with 10 g/L of tert-butanol was conducted. The latter is a well-known hydroxyl radical scavenger. The results are shown in Figure S1. Indeed, the vital role of hydroxyl radicals is indirectly confirmed since tert-butanol almost inhibited ANZ decomposition. The results are in agreement with several published works that demonstrate either the production of hydroxyl radicals by BDD using electron spin resonance spectroscopy [27] or a significant inhibition in the presence of hydroxyl radical scavengers [19].

A quasi-steady state can be assumed due to the lifetime of hydroxyl radicals, which is in the order of 10^{-9} s. As a result, Equation (2) can be written as follows [28]:

$$ -\frac{d[ANZ]}{dt} = k_{app}[ANZ] = k_{ANZ,HO^{\bullet}}[HO^{\bullet}][ANZ] \tag{3} $$

where $k_{ANZ,HO^{\bullet}}$ is the absolute rate constant.

Competition kinetics was applied to calculate the absolute kinetic constant. Benzoic acid (BA) was selected as the probe compound since the reaction between BA and hydroxyl radicals is well-studied, with a kinetic constant equal to 4.3×10^{9} M^{-1} s^{-1}, while BA is recalcitrant to direct anodic oxidation [28].

Therefore, the absolute constant can be estimated using the following equation:

$$ k_{ANZ,HO^{\bullet}} = k_{BA,HO^{\bullet}} \cdot \frac{k_{app,ANZ}}{k_{app,BA}} \tag{4} $$

Thus, using the ratio $k_{app,ANZ}/k_{ANZ,HO^{\bullet}}$, the concentration of hydroxyl radicals in steady state [·OH]ss can be calculated as being equal to 0.77×10^{-13} M for j = 12.5 mA/cm^2, 0.1 M Na$_2$SO$_4$, pH 7.

3.3. Effect of Initial Concentration

The effect of the initial ANZ concentration on its removal in 0.1 M Na$_2$SO$_4$ is shown in Figure 2. The k_{app} values of 0.022 and 0.0224 min^{-1} were computed for the removal of 0.5 and 1 mg L^{-1} of ANZ, respectively. From these almost equal k_{app} values, it is implied that the reaction indeed follows first-order kinetics at low ANZ concentrations, where the rate increases proportionately with the concentration of ANZ. At a concentration of 2 mg L^{-1}, the rate also increases with concentration, although this is not proportionate. However, data can perfectly fit into Equation (2); thus, degradation follows pseudo-first-order kinetics at higher initial concentrations. Similar results have been reported for the electrochemical degradation of different emerging contaminants, such as ethyl paraben [17], ampicillin [24], and thiamethoxam [23]. For a constant current density, the number of ROS generated remains constant, and therefore, the kinetics is completely dependent on the concentration of ANZ and/or mass transfer. These results strongly suggest that the initial concentration of the organic pollutant plays a significant role in determining the degradation kinetics. It is necessary to work with environmentally relevant concentrations of ANZ to avoid the misrepresentation of the degradation kinetics.
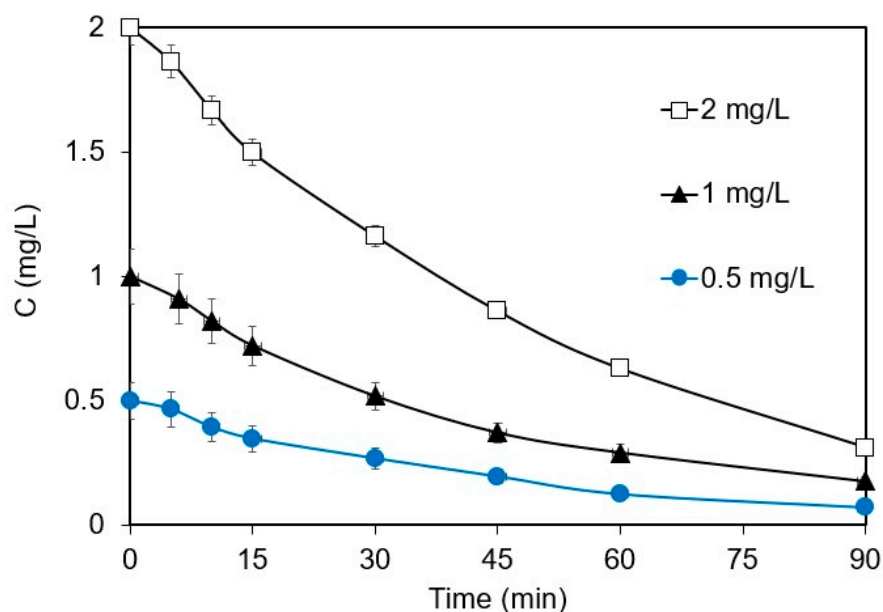
Figure 2. Effect of initial concentration on the removal of ANZ at j = 6.25 mA cm^{-2} (galvanostatic conditions), [Na$_2$SO$_4$] = 0.1 M, and pH = 6.2.

3.4. Effect of Supporting Electrolytes

The effect of the type of electrolyte on the removal of 1 mg L^{-1} was studied using 0.1 M Na$_2$SO$_4$ or 0.1 M NaCl, and the results are shown in Figure 3a. The removal is favored in the presence of Na$_2$SO$_4$, with the respective k$_{app}$ value of 0.0224 min^{-1} being nearly twice as much (0.0132 min^{-1}) as that with NaCl. The formation of sulfate ROS, such as S$_2$O$_8^-$ and SO$_4^-$· ions, facilitates the removal of ANZ. Similar results have been reported for the degradation of florfenicol [29]. The role of chloride in the electrochemical removal of ANZ will be discussed in detail in Section 3.6. Furthermore, the effect of electrolyte concentrations on the ANZ is evaluated and shown in Figure 3b.
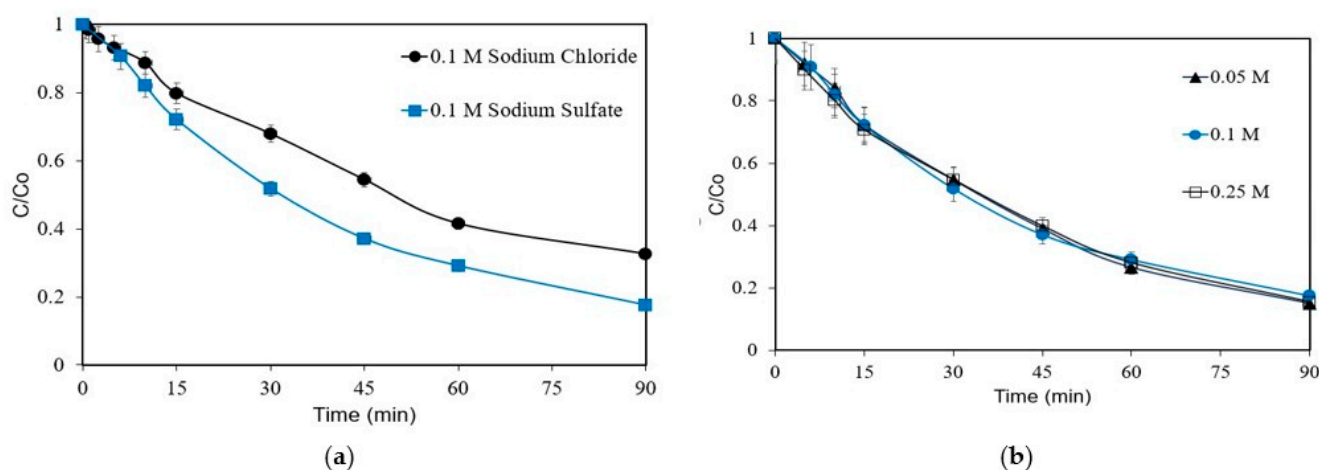

(a)

(b)

Figure 3. Removal of ANZ as a function of (**a**) electrolyte type and (**b**) Na$_2$SO$_4$ concentration for [ANZ]$_o$ = 1 mg L^{-1}, j = 6.25 mA cm^{-2} (galvanostatic conditions), and pH = 6.2.

As can be seen, there is no significant impact of the electrolyte concentration on the removal of ANZ. Similar results were reported for the anodic oxidation of 2,4-dichlorophenoxyacetic acid, where the electrolyte concentration did not influence the compound's removal [30]. Another work investigating the degradation of dye X-6G showed an almost similar removal for Na$_2$SO$_4$ concentrations varying between 0.025 and 0.1 M [31]. The removal of ANZ is most likely to be directly proportional to the number of ·OH radicals

generated within the system. As this remains almost constant with the operating conditions, the electrolyte concentration has no significant effect on the removal of ANZ.

3.5. Effect of pH

Experiments were performed with 1 mg L^{-1} of ANZ in 0.1 M Na$_2$SO$_4$ to assess the influence of pH in the range of 3–10 on ANZ degradation. There is no significant change when the initial pH increases from its inherent value of 6.2 to 10 (Figure 4). However, ANZ removal increases when the pH is reduced to acidic conditions, i.e., the respective k$_{app}$ increases from 0.0224 to 0.0394 min^{-1} upon reducing pH from 6.2 to 3. The formation of ·OH radicals on the surface of the BDD electrode is typically favored in an acidic environment, and so is their oxidation potential. In a study on the degradation of tetracycline, k$_{app}$ increased slightly upon decreasing the solution pH from 9 to 3 [32]. Many studies involving electrochemical oxidation over BDD have shown that the influence of pH within a range of 2–9 on the apparent rate constant values is not noteworthy [17,33,34].
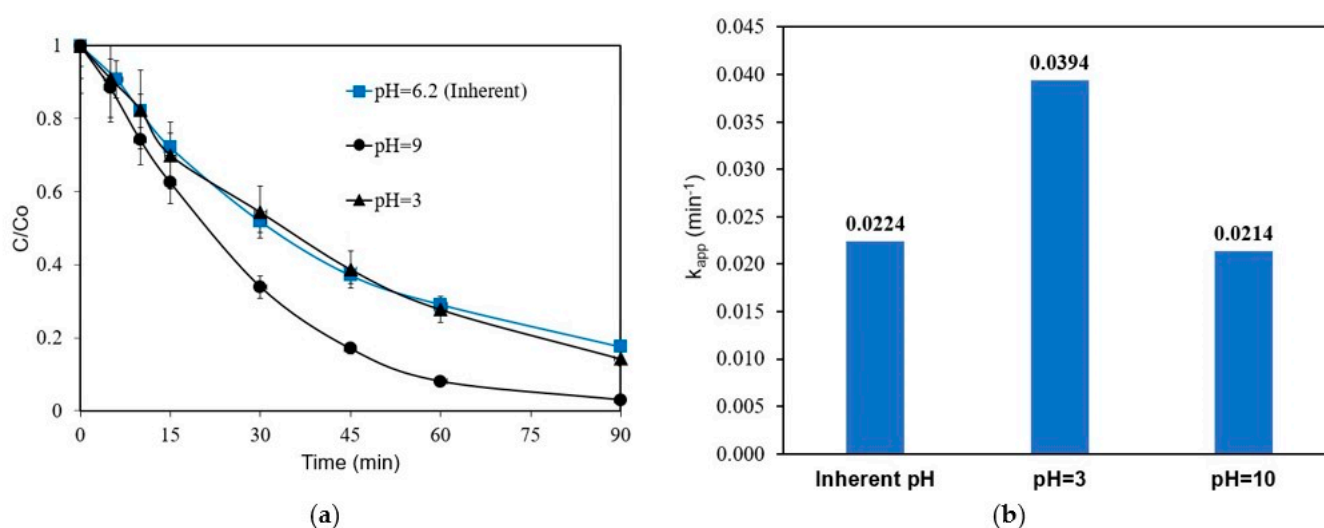

Figure 4. Effect of initial solution pH on ANZ removal (**a**) concentration profiles and (**b**) k$_{app}$ values for [ANZ]$_o$ = 1 mg L^{-1}, [Na$_2$SO$_4$] = 0.1 M, and j = 6.25 mA cm^{-2} (galvanostatic conditions).

It should be mentioned that the solution pH was adjusted but not buffered to its initial value. However, it remained quite stable throughout the experiment, i.e., the final value was 9.7 for the experiment in alkaline conditions and 3.9 for the experiment in acidic conditions.

3.6. Effect of the Water Matrix

All the experiments described so far were performed in ultrapure water (UPW) containing zero organics (i.e., <50 μgL^{-1} total organic carbon). Further experiments were performed in bottled water (BW) and real hospital wastewater effluent (WW), with the addition of 0.1 M Na$_2$SO$_4$, and the results are presented in Figure 5a. Removal is slightly reduced from 82.5% in UPW to 79.7% and 74.7% in BW and WW, respectively. This reduction may be attributed to the interference of other inorganic ions and organic matter inherently present in these water matrices. For instance, inorganics could lead to the generation of different secondary oxidants, which could either accelerate degradation or scavenge other radicals contributing to the degradation; the first phenomenon is presumably beneficial, while the second is detrimental. Therefore, and due to the uncertainty regarding the influence of the water matrix, the degradation of ANZ at different water compositions was evaluated.
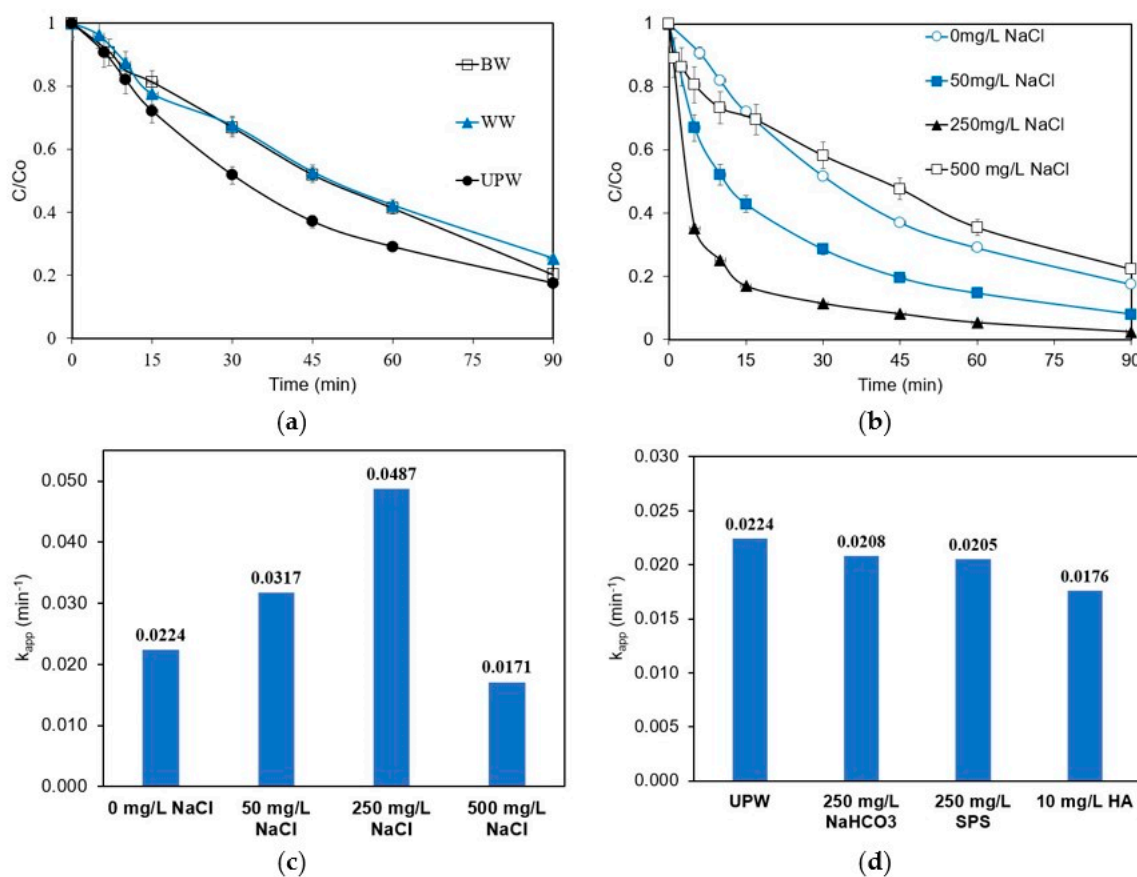
Figure 5. Removal of ANZ as a function of (**a**) the actual water matrix, (**b**,**c**) chloride added in UPW at various concentrations, and (**d**) various water constituents added in UPW for $[ANZ]_o = 1$ mg L^{-1}, $[Na_2SO_4] = 0.1$ M, $j = 6.25$ mA cm^{-2} (galvanostatic conditions), and pH = 6.

Figure 5b shows the effect of the addition of chloride on the removal of ANZ. The addition of chloride up to 250 mg L^{-1} has a positive influence on the system, increasing the k_{app} values from 0.0224 min^{-1} in the absence of chloride to 0.0317 and 0.0487 min^{-1} for chloride concentrations of 50 and 250 mg L^{-1}, respectively (Figure 5c). In the presence of chloride, chlorine is electro-generated at the surface of the anode, according to Equation (5), and eventually yields two strong oxidants, HOCl and ClO$^-$, as shown in Equations (6) and (7).

$$2Cl^- \rightarrow Cl_2 + 2e^- \tag{5}$$

$$Cl_2 + H_2O \Leftrightarrow HOCl + H^+ + Cl^- \tag{6}$$

$$HOCl \Leftrightarrow ClO^- + H^+ \tag{7}$$

These active chlorine species contribute to the indirect oxidation of ANZ; however, on further increasing the concentration of chloride to 500 mg L^{-1}, an adverse effect is observed. The k_{app} value decreases to 0.0171 min^{-1}, lower than that found in the absence of chloride. The presence of both ·OH and Cl$^-$ at the surface of BDD leads to the scavenging of ·OH radicals by Cl$^-$. The reaction between the two forms of ClO$^-$ further consumes ·OH to form ClO$_2^-$, ClO$_3^-$, and ClO$_4^-$. Similar results have been reported for the removal of organo-phosphorous pesticides [35]. These results also support the reduced ANZ removal reported in this work, using 0.1 M NaCl as the supporting electrolyte.

The effect of adding bicarbonate, sodium persulfate (SPS), or humic acid (HA) is shown in Figure 5d in terms of the respective apparent rates. Their impact is rather inconsiderable

(although slightly negative) and can be explained as follows: in the presence of bicarbonate, carbonate radicals are formed as per Equations (8) and (9).

$$CO_3^{2-} + \cdot OH \Leftrightarrow CO_3^- \cdot + HO^- \tag{8}$$

$$HCO_3^- + \cdot OH \Leftrightarrow CO_3^- \cdot + H_2O \tag{9}$$
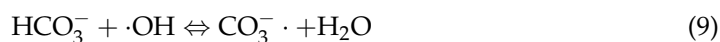
Carbonate radicals are weaker oxidants and trap the powerful hydroxyl radicals, explaining the lower removal rate of ANZ. Similar effects have also been reported for the electrochemical removal of dexamethazone [36] and acephate [35]. The addition of HA mimics the organic carbon present in wastewater or environmental samples. In the presence of 10 mg L^{-1} HA, the 90-min removal is slightly reduced from 82.4% to 79.8% (removal data are not shown). HA may block the active sites on the electrodes and consequently compete for the generated ROS. The same effect has been reported for the electrochemical abatement of diclofenac [37] and ampicillin [24].

Persulfate can be activated according to Equation (10):

$$S_2O_8^- + e^- \rightarrow SO_4^- \cdot + SO_4^{2-} \tag{10}$$

Several studies have reported the efficient removal of pollutants by combining electrochemical oxidation and the electrochemical activation of persulfate. The combined effect of $\cdot OH$ and $SO_4^- \cdot$ radicals helps in the faster removal of the pollutants. Such combined effects were reported for the removal of sulfamethazine [38], atrazine [39], and bisphenol A [40], among many other compounds. However, no significant improvement in ANZ removal is observed in this work in the conditions studied, suggesting that the removal probably occurs only by $\cdot OH$ radicals, as already discussed in Section 3.2.

3.7. Energy Consumption and Cost Analysis

The industrial implementation of any technology depends on the economic feasibility of the process, which, in turn, is usually determined by its energy consumption. Therefore, the energy requirement is a key parameter that is always considered before the practical application of a proposed technology on a large scale. Energy consumption can be estimated by the term electric energy per order (EEO), coined by Bolton et al. [41]. The EEO is defined as the electrical energy required to reduce the concentration of a parent compound by an order of magnitude per cubic meter of wastewater. For a batch reactor, the EEO can be written as Equation (11).

$$EEO = \frac{P \times t \times 1000}{V \, \log\left(\frac{C_o}{C_f}\right)} \tag{11}$$

where EEO is the electrical energy (kWh), P is the power consumption of the system (kW), t is the treatment time (h), V is the volume of the wastewater (L), and C_o and C_f are the initial and final concentrations of the target compound before and after treatment, respectively. By assuming first-order kinetics and the apparent rate constant k_{app} in min^{-1}, simplifying Equation (11) yields

$$EEO = \frac{38.38 \, P}{V \, k_{app}} \tag{12}$$

Applying Equation (12) to the electrochemical removal of ANZ in 0.1 M Na$_2$SO$_4$ at j = 6.25 mA cm^{-2} and j = 12.5 mA cm^{-2}, EEO values of 23.1 and 25 kWhm^{-3}/order are respectively computed. The average electricity prices in the EU for the second half of 2021 were reported to be 0.14 €/kWh for non-household customers [42]. Using these average prices, the process cost in terms of the EEO is calculated as 3.3 and 3.6 € m^{-3}/order for j = 6.25 mA cm^{-2} and j = 12.5 mA cm^{-2}, respectively.

3.8. Electrochemical Oxidation versus Solar Photo-Fenton

The only other study reporting the removal of ANZ was carried out using the solar photo-Fenton process [20]. In that work, the researchers studied ANZ removal in two different water matrices, i.e., UPW and hospital wastewater. For an optimized ANZ concentration of 0.05 mg L^{-1}, the removal efficiency was 95% in UPW and 51% in wastewater in about 70 min. However, when the concentration of ANZ increased to 0.5 mg L^{-1} in UPW, ANZ removal was around 85% in 120 min, with H_2O_2 and Fe^{2+} concentrations of 50 and 5 mg L^{-1}, respectively. They also reported that the degradation of ANZ followed pseudo-first-order kinetics.

Those results are also comparable to the electrochemical degradation of ANZ, where 85% of ANZ at an initial concentration of 0.5 mg L^{-1} was removed in 90 min. The electrochemical oxidation of ANZ was slightly favored at a reduced pH. However, it remained almost unaltered upon increasing the pH to 10, indicating that the EO process could be carried out for a wide pH range. On the contrary, the solar photo-Fenton process needed a pH adjustment to 5 to facilitate the Fenton reaction, which could be a significant limitation when dealing with real industrial effluents and environmental matrices as the inherent pH of most industrial effluent lies in the neutral to basic range. Comparing these two processes in terms of economic feasibility might be complex, involving several considerations. Although EO is pH-independent, the process's energy consumption is larger than the solar photo-Fenton process. The continuous availability of sunlight and the cost of the chemicals used in the Fenton process are the driving factors behind its economic feasibility.

4. Conclusions

The breast-cancer drug anastrozole was removed in environmentally relevant concentrations using electrochemical oxidation on a BDD electrode. The influence of various operating conditions, such as current density, pH, initial ANZ concentration, and the nature of the electrolytes, was investigated alongside the water matrix, where this emerging contaminant is typically found. The influence of chloride on ANZ abatement is significant and can be either positive at lower concentrations or detrimental at higher ones. The beneficial role of increasing current density seems to be the most vital parameter in the performance of the entire process. However, the direct correlation between current density and energy consumption can be considered the main limitation of this process. Other process parameters have no significant impact on ANZ degradation. The addition of another oxidant, such as persulfate, has no positive effect on the process. It implies that ANZ degradation might be rather selective to $\cdot$OH radicals compared to $SO_4{}^-\cdot$ radicals. ANZ electrochemical oxidation is more viable in the long run due to the lack of chemical additions and the wide range of operating parameters, unlike other AOPs that may require a constant light source, specific pH, or catalyst addition. A preliminary cost analysis shows that the process economics is directly proportional to the energy cost. Cleaner and renewable sources of electricity generation, however, could make the process more economically feasible in the future, as the prices of energy from renewable sources are expected to fall drastically in the coming decades.

Data Availability Statement: The data presented in this study are available on request from the corresponding author.

Conflicts of Interest: The authors declare no conflict of interest.

References

1. Bray, F.; Ferlay, J.; Soerjomataram, I.; Siegel, R.L.; Torre, L.A.; Jemal, A. Global cancer statistics 2018: GLOBOCAN estimates of incidence and mortality worldwide for 36 cancers in 185 countries. *CA A Cancer J. Clin.* **2018**, *68*, 394–424. [CrossRef] [PubMed]
2. WHO. *Breast Cancer Factsheets*; WHO: Geneva, Switzerland, 2021.
3. Ghadge, D.; Nangare, S.; Jadhav, N. Formulation, optimization, and in vitro evaluation of anastrozole-loaded nanostructured lipid carriers for improved anticancer activity. *J. Drug Deliv. Sci. Technol.* **2022**, *72*, 103354. [CrossRef]
4. Evaluation of Pharmacokinetics and Safety with Bioequivalence of Anastrozole in Healthy Chinese Volunteers. *Clin. Pharmacol. Drug Dev.* **2022**, *11*, 687–694. [CrossRef]
5. WHO. *World Health Organization Model List of Essential Medicines: 21st list 2019*; Technical documents; WHO: Geneva, Switzerland, 2019.
6. Lonning, P.; Pfister, C.; Martoni, A.; Zamagni, C. Pharmacokinetics of third-generation aromatase inhibitors. *Semin. Oncol.* **2003**, *30*, 23–32. [CrossRef]
7. ClinCalc DrugStats Database. *Clin. Pharmacol. Drug Dev.* **2022**, *8*. Available online: https://clincalc.com/DrugStats/Drugs/Anastrozole (accessed on 23 September 2022).
8. Wilkinson, K. Anastrozole (ArimidexR). *Home Clin. J. Oncol. Nurs.* **2004**, *8*, 87–88. [CrossRef]
9. Tousova, Z.; Oswald, P.; Slobodnik, J.; Blaha, L.; Muz, M.; Hu, M.; Brack, W.; Krauss, M.; Di Paolo, C.; Tarcai, Z.; et al. European demonstration program on the effect-based and chemical identification and monitoring of organic pollutants in European surface waters. *Sci. Total Environ.* **2017**, *601–602*, 1849–1868. [CrossRef]
10. Liu, X.; Zhang, J.; Yin, J.; Duan, H.; Wu, Y.; Shao, B. Analysis of hormone antagonists in clinical and municipal wastewater by isotopic dilution liquid chromatography tandem mass spectrometry. *Anal. Bioanal. Chem.* **2010**, *396*, 2977–2985. [CrossRef]
11. Chen, L.; Yang, S.; Zuo, X.; Huang, Y.; Cai, T.; Ding, D. Biochar modification significantly promotes the activity of Co_3O_4 towards heterogeneous activation of peroxymonosulfate. *Chem. Eng. J.* **2018**, *354*, 856–865. [CrossRef]
12. Oturan, M.A. Outstanding performances of the BDD film anode in electro-Fenton process: Applications and comparative performance. *Curr. Opin. Solid State Mater. Sci.* **2021**, *25*, 100925. [CrossRef]
13. Ganzenko, O.; Trellu, C.; Oturan, N.; Huguenot, D.; Pechaud, Y.; van Hullebusch, E.D.; Oturan, M.A. Electro-Fenton treatment of a complex pharmaceutical mixture: Mineralization efficiency and biodegradability enhancement. *Chemosphere* **2020**, *253*, 126659. [CrossRef] [PubMed]
14. Nidheesh, P.; Zhou, M.; Oturan, M.A. An overview on the removal of synthetic dyes from water by electrochemical advanced oxidation processes. *Chemosphere* **2018**, *197*, 210–227. [CrossRef] [PubMed]
15. Brillas, E.; Martinez-Huitle, C.A. Decontamination of wastewaters containing synthetic organic dyes by electrochemical methods. An updated review. *Appl. Catal. B Environ.* **2015**, *166–167*, 603–643. [CrossRef]
16. Bampos, G.; Petala, A.; Frontistis, Z. Recent Trends in Pharmaceuticals Removal from Water Using Electrochemical Oxidation Processes. *Environments* **2021**, *8*, 85. [CrossRef]
17. Frontistis, Z.; Antonopoulou, M.; Yazirdagi, M.; Kilinc, Z.; Konstantinou, I.; Katsaounis, A.; Mantzavinos, D. Boron-doped diamond electrooxidation of ethyl paraben: The effect of electrolyte on by-products distribution and mechanisms. *J. Environ. Manag.* **2017**, *195*, 148–156. [CrossRef]
18. Peckova, K.; Musilova, J.; Barek, J. Boron-Doped Diamond Film Electrodes—New Tool for Voltammetric Determination of Organic Substances. *Crit. Rev. Anal. Chem.* **2009**, *39*, 148–172. [CrossRef]
19. Pueyo, N.; Ormad, M.P.; Miguel, N.; Kokkinos, P.; Ioannidi, A.; Mantzavinos, D.; Frontistis, Z. Electrochemical oxidation of butyl paraben on boron doped diamond in environmental matrices and comparison with sulfate radical-AOP. *J. Environ. Manag.* **2020**, *269*, 110783. [CrossRef]
20. Sanabria, P.; Scunderlick, D.; Wilde, M.L.; Ludtke, D.S.; Sirtori, C. Solar photo-Fenton treatment of the anti-cancer drug anastrozole in different aqueous matrices at near-neutral pH: Transformation products identification, pathways proposal, and in silico (Q)SAR risk assessment. *Sci. Total Environ.* **2021**, *754*, 142300. [CrossRef]
21. Fotouhi, L.; Hashkavayi, A.B.; Heravi, M.M. Electrochemical behaviour and voltammetric determination of sulphadiazine using a multi-walled carbon nanotube composite film-glassy carbon electrode. *J. Exp. Nanosci.* **2013**, *8*, 947–956. [CrossRef]
22. Feijoo, S.; Kamali, M.; Pham, Q.K.; Assoumani, A.; Lestremau, F.; Cabooter, D.; Dewil, R. Electrochemical Advanced Oxidation of Carbamazepine: Mechanism and optimal operating conditions. *Chem. Eng. J.* **2022**, *446*, 137114. [CrossRef]
23. Lebik-Elhadi, H.; Frontistis, Z.; Ait-Amar, H.; Amrani, S.; Mantzavinos, D. Electrochemical oxidation of pesticide thiamethoxam on boron doped diamond anode: Role of operating parameters and matrix effect. *Process Saf. Environ. Prot.* **2018**, *116*, 535–541. [CrossRef]
24. Frontistis, Z.; Mantzavinos, D.; Meric, S. Degradation of antibiotic ampicillin on boron-doped diamond anode using the combined electrochemical oxidation—Sodium persulfate process. *J. Environ. Manag.* **2018**, *223*, 878–887. [CrossRef] [PubMed]

25. Kaur, R.; Kushwaha, J.P.; Singh, N. Amoxicillin electro-catalytic oxidation using Ti/RuO$_2$ anode: Mechanism, oxidation products and degradation pathway. *Electrochim. Acta* **2019**, *296*, 856–866. [CrossRef]

26. De Luna, Y.; Bensalah, N. Review on the electrochemical oxidation of endocrine-disrupting chemicals using BDD anodes. *Curr. Opin. Electrochem.* **2022**, *32*, 100900. [CrossRef]

27. Marselli, B.; Garcia-Gomez, J.; Michaud, P.-A.; Rodrigo, M.A.; Comninellis, C. Electrogeneration of Hydroxyl Radicals on Boron-Doped Diamond Electrodes. *J. Electrochem. Soc.* **2003**, *150*, D79. [CrossRef]

28. Arvaniti, O.S.; Konstantinou, I.; Mantzavinos, D.; Frontistis, Z. Destruction of valsartan using electrochemical and electrochemical/persulfate process. Kinetics, identification of degradation pathway and application in aqueous matrices. *J. Environ. Chem. Eng.* **2021**, *9*, 106265. [CrossRef]

29. Periyasamy, S.; Lin, X.; Ganiyu, S.O.; Kamaraj, S.K.; Thiam, A.; Liu, D. Insight into BDD electrochemical oxidation of florfenicol in water: Kinetics, reaction mechanism, and toxicity. *Chemosphere* **2022**, *288*, 132433. [CrossRef] [PubMed]

30. Cai, J.; Zhou, M.; Pan, Y.; Lu, X. Degradation of 2,4-dichlorophenoxyacetic acid by anodic oxidation and electro-Fenton using BDD anode: Influencing factors and mechanism. *Sep. Purif. Technol.* **2020**, *230*, 115867. [CrossRef]

31. Tang, Y.; He, D.; Guo, Y.; Qu, W.; Shang, J.; Zhou, L.; Pan, R.; Dong, W. Electrochemical oxidative degradation of X-6G dye by boron-doped diamond anodes: Effect of operating parameters. *Chemosphere* **2020**, *258*, 127368. [CrossRef]

32. Frontistis, Z.; Meric, S. The role of operating parameters and irradiation on the electrochemical degradation of tetracycline on boron doped diamond anode in environmentally relevant matrice. *J. Chem. Technol. Biotechnol.* **2018**, *93*, 3648–3655. [CrossRef]

33. El-Ghenymy, A.; Arias, C.; Cabot, P.L.; Centellas, F.; Garrido, J.A.; Rodriguez, R.M.; Brillas, E. Electrochemical incineration of sulfanilic acid at a boron-doped diamond anode. *Chemosphere* **2012**, *87*, 1126–1133. [CrossRef]

34. Pereira, G.F.; Rocha-Filho, R.C.; Bocchi, N.; Biaggio, S.R. Electrochemical degradation of bisphenol A using a flow reactor with a boron-doped diamond anode. *Chem. Eng. J.* **2012**, *198–199*, 282–288. [CrossRef]

35. Ning, Y.; Li, K.; Zhao, Z.; Chen, D.; Li, Y.; Liu, Y.; Yang, Q.; Jiang, B. Simultaneous electrochemical degradation of organophosphorus pesticides and recovery of phosphorus: Synergistic effect of anodic oxidation and cathodic precipitation. *J. Taiwan Inst. Chem. Eng.* **2021**, *125*, 267–275. [CrossRef]

36. Grilla, E.; Taheri, M.E.; Miserli, K.; Venieri, D.; Konstantinou, I.; Mantzavinos, D. Degradation of dexamethasone in water using BDD anodic oxidation and persulfate: Reaction kinetics and pathways. *J. Chem. Technol. Biotechnol.* **2021**, *196*, 2451–2460. [CrossRef]

37. Giannakopoulos, S.; Kokkinos, P.; Hasa, B.; Frontistis, Z.; Katsaounis, A.; Mantzavinos, D. Electrochemical Oxidation of Pharmaceuticals on a Pt–SnO2/Ti Electrode. *Electrocatalysis* **2022**, *13*, 363–377. [CrossRef]

38. Nashat, M.; Mossad, M.; El-Etriby, H.K.; Gar Alalm, M. Optimization of electrochemical activation of persulfate by BDD electrodes for rapid removal of sulfamethazine. *Chemosphere* **2022**, *286*, 131579. [CrossRef]

39. Bu, L.; Zhu, S.; Zhou, S. Degradation of atrazine by electrochemically activated persulfate using BDD anode: Role of radical and influencing factors. *Chemosphere* **2018**, *195*, 236–244. [CrossRef] [PubMed]

40. Ding, J.; Bu, L.; Zhao, Q.; Kabutey, F.T.; Wei, L.; Dionysiou, D.D. Electrochemical activation of persulfate on BDD and DSA anodes: Electrolyte influence, kinetics and mechanisms in the degradation of bisphenol A. *J. Hazard. Mater.* **2020**, *388*, 121789. [CrossRef]

41. Bolton, J.R.; Bircher, K.G.; Tumas, W.; Tolman, C.A. Figures-of-merit for the technical development and application of advanced oxidation technologies for both electric- and solar-driven systems (IUPAC Technical Report). *Pure Appl. Chem.* **2001**, *73*, 627–637. [CrossRef]

42. Eurostat. *Electricity Price Statistics*; Eurostat Statistics Explained; Eurostat: Luxemburg, 2022.